



Quaternary diborides—improving the oxidation resistance of $TiB_{2\pm z}$ coatings by disilicide alloying

Ahmed Bahr, Oskar Beck, Thomas Glechner, Alexander Grimmer, Tomasz Wojcik, Philip Kutrowatz, Jürgen Ramm, Oliver Hunold, Szilard Kolozsvári, Peter Polcik, Eleni Ntemou, Daniel Primetzhofer & Helmut Riedl

To cite this article: Ahmed Bahr, Oskar Beck, Thomas Glechner, Alexander Grimmer, Tomasz Wojcik, Philip Kutrowatz, Jürgen Ramm, Oliver Hunold, Szilard Kolozsvári, Peter Polcik, Eleni Ntemou, Daniel Primetzhofer & Helmut Riedl (2023) Quaternary diborides—improving the oxidation resistance of $TiB_{2\pm z}$ coatings by disilicide alloying, Materials Research Letters, 11:9, 733-741, DOI: [10.1080/21663831.2023.2225554](https://doi.org/10.1080/21663831.2023.2225554)

To link to this article: <https://doi.org/10.1080/21663831.2023.2225554>



© 2023 The Author(s). Published by Informa UK Limited, trading as Taylor & Francis Group



[View supplementary material](#)



Published online: 26 Jun 2023.



[Submit your article to this journal](#)



[View related articles](#)



[View Crossmark data](#)

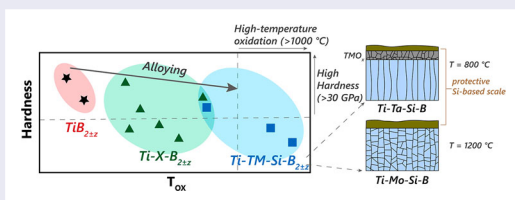
Quaternary diborides—improving the oxidation resistance of $\text{TiB}_{2\pm z}$ coatings by disilicide alloying

Ahmed Bahr ^a, Oskar Beck ^a, Thomas Glechner ^a, Alexander Grimmer^a, Tomasz Wojcik ^a, Philip Kutrowatz^a, Jürgen Ramm ^b, Oliver Hunold ^b, Szilard Kolozsvári ^c, Peter Polcik ^c, Eleni Ntemou ^d, Daniel Primetzhofer ^d and Helmut Riedl ^{a,e}

^aChristian Doppler Laboratory for Surface Engineering of high-performance Components, TU Wien, Vienna, Austria; ^bOerlikon Balzers, Oerlikon Surface Solutions AG, Balzers, Liechtenstein; ^cPlansee Composite Materials GmbH, Lechbruck am See, Germany; ^dDepartment of Physics and Astronomy, Uppsala University, Uppsala, Sweden; ^eInstitute of Materials Science and Technology, TU Wien, Vienna, Austria

ABSTRACT

To overcome the limited oxidation resistance of the emerging class of transition metal borides, we suggest within this study novel quaternary diborides, $\text{Ti-TM-Si-B}_{2\pm z}$ ($\text{TM} = \text{Ta}, \text{Mo}$), achieving the compromise between excellent oxidation resistance and requirements of hard coatings. Single-phase AlB_2 -type structured $\text{Ti-TM-Si-B}_{2\pm z}$ films ($3\text{--}5\ \mu\text{m}$) are sputter-deposited from $\text{TiB}_2/\text{TMSi}_2$ targets. The $\text{Ti-Ta-Si-B}_{2\pm z}$ coatings exhibit 36 GPa in hardness, while maintaining strongly retarded oxidation kinetics till 1000°C . $\text{Ti-Mo-Si-B}_{2\pm z}$ coatings preserve a hardness up to 27 GPa, although outperforming all their counterparts by featuring outstanding oxidation resistance with 440 nm oxide scale thickness after 1 h at 1200°C .



IMPACT STATEMENT

First report on quaternary $\text{Ti-TM-Si-B}_{2\pm z}$ coatings stabilized in hexagonal AlB_2 -prototype structures. These hard coating materials exhibit unprecedented oxidation resistance up to 1200°C due to the formation of Si-rich scales.

ARTICLE HISTORY

Received 27 March 2023

KEYWORDS

Titanium diboride; sputtering; thin films; oxidation resistance; UHTC; Disilicides

1. Introduction

Boron based thin film materials are subject of growing research interests and considered as potential future protective and functional coatings applied in diverse applications ranging from energy production to aerospace or cutting tool industry [1–9]. Within the interesting family of transition metal diborides (TMB_2), $\text{TiB}_{2\pm z}$ exhibits an attractive aggregate of properties with high thermal stability ($T_M \sim 3225^\circ\text{C}$), super-hardness ($> 40\ \text{GPa}$), low density, but also good thermal and electrical conductivity accompanied by chemical inertness [1,5,10–15]. However, still one of the major obstacles against the wide applicability of $\text{TiB}_{2\pm z}$ based films is their limited oxidation resistance above 400°C [16–18].

The oxidation behavior for $\text{TiB}_{2\pm z}$ bulk and thin film materials has been extensively studied [16,17,19–22], and features specific morphological and kinetic-related aspects. According to Cai et al., monolithic bulk TiB_2 starts to oxidize at 400°C , whereas a rapid, anomalous oxidation sets in at around 500°C . The reported accelerated oxidation at 500°C is related to the formation of an outer mixed amorphous/crystalline $\text{B}_2\text{O}_3/\text{TiO}_2$ scale, and an inner unstable Ti-B-O layer [21]. Between 650°C and 1000°C —also referred as the low-temperature regime—the scale formation changes to a laminated configuration with crystalline TiO_2 and a glassy amorphous B_2O_3 providing a certain oxidation resistance [19–22]. At higher temperatures, the accelerated kinetics

CONTACT Ahmed Bahr ahmed.bahr@tuwien.ac.at Christian Doppler Laboratory for Surface Engineering of high-performance Components, TU Wien, Vienna A-1060, Austria

Supplemental data for this article can be accessed here. <https://doi.org/10.1080/21663831.2023.2225554>

© 2023 The Author(s). Published by Informa UK Limited, trading as Taylor & Francis Group.

This is an Open Access article distributed under the terms of the Creative Commons Attribution License (<http://creativecommons.org/licenses/by/4.0/>), which permits unrestricted use, distribution, and reproduction in any medium, provided the original work is properly cited. The terms on which this article has been published allow the posting of the Accepted Manuscript in a repository by the author(s) or with their consent.

predominates the oxidation process, forming volatile B_2O_3 accompanied by non-protective porous TiO_2 scales [19,23,24]. However, this oxidation sequence is reported to be different for $TiB_{2\pm z}$ -based thin film materials. Huang et al. highlighted the formation of the B_2O_3 (l) phase, evolving volatile at around $720^\circ C$, and hence results in a rapid oxidation of their chemical vapor deposited TiB_2 coating [22]. In contrast, the oxidation of physical vapor deposited (PVD) $TiB_{2\pm z}$ below $800^\circ C$ in air did not exhibit the formation of B_2O_3 (l), and the oxide scales have been reported to be Ti-rich [16–18]. Thörnberg et al. indicated that the B concentration plays a prominent role on the oxidation kinetics of sputtered $TiB_{2\pm z}$ thin films [16]. Their sub-stoichiometric $TiB_{1.43}$ films exhibited lower oxidation rates compared to the B-rich films, due to the absence of the rapidly oxidizing B-rich tissue phases. Nevertheless, all their investigated $TiB_{2\pm z}$ films follow linear-rate laws with low oxidation resistance over $400^\circ C$ [16].

Different routes have been attempted to enhance the oxidation resistance of $TiB_{2\pm z}$ coatings mainly based on alloying with strong oxide formers such as Al [18,25,26] or Si [27,28]—which are prone to form protective oxide scales. Bakhit et al. reported an improvement in the oxidation resistance of sputtered $Ti_{0.68}Al_{0.32}B_{1.35}$ with retarded kinetics at $800^\circ C$ for 0.5 h, due to the formation of a dense Al-based oxide scale of 470 nm compared to a scale thickness of 1900 nm obtained for their binary $TiB_{2.4}$ counterpart [18]. Recently, Navidi et al. followed the Al-alloying strategy to deposit Al-rich but nearly stoichiometric $(Ti_{0.35}Al_{0.65})B_2$ films revealing an outstanding oxidation resistance at $700^\circ C$ by forming a thin Al-based oxide scale of only 39 ± 7 nm after 8 h [25]. The high Al-content predominates the oxidation behavior, but on the expense of the mechanical properties with reported hardness between 9 and 24 GPa [25]. The influence of Si-alloying on the oxidation resistance of several $TiB_{2\pm z}$ based coatings was studied by Glechner et al. [27]. For Ti-Si- $B_{2\pm z}$ coatings, the Si addition provided high-temperature oxidation resistance with strongly retarded kinetics up to $1200^\circ C$, while the reported hardness drastically decreased upon high-Si content addition to a value around 16 GPa [27]. Still, the above-mentioned alloying routes by Al and Si to form oxidation-resistant ternary diborides are limited by the deterioration of the coatings' mechanical properties. For bulk refractory diborides, a different strategy is followed to enhance the oxidation resistance. Through the addition of secondary Si-based phases (i.e. SiC or $TMSi_2$), which minorly influence the desired mechanical properties, highly protective glassy-like borosilicate scales can be formed [23,29–34]. A similar approach has been also applied for Zr-Mo-Si-B based-coatings to

provide high-temperature oxidation resistance [35,36]. Merging now these ideas to form quaternary, hexagonal structured diboride-based thin film materials by alloying $TMSi_2$ phases into binary $TiB_{2\pm z}$ is a promising—yet relatively unexplored—strategy offering new possibilities to achieve the challenging compromise between good mechanical properties and highest oxidation resistance.

To prove the suggested concept, this study explores the alloying of physical vapor deposited $TiB_{2\pm z}$ coatings with $TMSi_2$ based phases (TM = Ti, Mo, Ta) grown from $TiB_2/TMSi_2$ compound target materials with various compositions— $TiB_2/TiSi_2$ (90/10 and 80/20 mol%), $TiB_2/TaSi_2$ (90/10 and 80/20 mol%), and $TiB_2/MoSi_2$ (85/15, 80/20 and 70/30 mol%).

2. Materials and methods

All the ternary and quaternary Ti-TM-Si- $B_{2\pm z}$ coating materials have been deposited in a laboratory-scale magnetron sputtering system using 3-inch sized target materials from Plansee Composite Materials GmbH. Each of the seven targets was solely DC-sputtered at a target current of 0.5 A in pure argon atmosphere (working pressure of 0.4 Pa). Additionally, a binary $TiB_{2.57}$ coating was deposited from a TiB_2 target at a pressure of 0.56 Pa. The coatings were grown onto sapphire and single-crystalline Si substrates (10 $\bar{1}$ -oriented, $10 \times 10 \times 0.53$ mm³ and 100-oriented, $20 \times 7 \times 0.38$ mm³) as well as poly-crystalline Al_2O_3 ($20 \times 7 \times 0.38$ mm³). The obtained film thicknesses of the quaternary Ti-TM-Si- $B_{2\pm z}$ coatings were in the range between 3.2 and 4.9 μm .

The chemical composition of the coatings was determined by ion beam analysis techniques using Time-of-Flight Elastic Recoil Detection Analysis (ToF-ERDA) and Rutherford Backscattering Spectrometry (RBS) at the 5 MV Pelletron Tandem accelerator laboratory at Uppsala University [37]. For ToF-ERDA, $^{127}I^{8+}$ projectiles with a primary energy of 36 MeV were employed with an incident angle of 67.5° with respect to the surface normal and a recoil detection angle of 45° . RBS was carried out using 3 MeV $^4He^+$ ions and a detection angle of 170° . The analysis of the ToF-ERDA experimental data was performed using the Potku software [38], while the RBS data were analyzed using the SIMNRA software [39]. The total systematic and statistical uncertainties were estimated to be 5–8% of the deduced value for the major constituents.

The oxidation behavior of the coatings was investigated using DTA/TG system (Netzsch STA 449 F1). The dynamic measurements up to $1400^\circ C$ were done at a heating rate of $10^\circ C/min$, under flowing synthetic air (50 ml/min) and helium (20 ml/min). The employed samples for these measurements were the

coated polycrystalline Al_2O_3 . Further isothermal annealing measurements were done in ambient air using conventional furnace at 800°C and 1200°C. Moreover, the mechanical properties of the coatings were investigated using an ultra-micro indentation (UMIS) system equipped with Berkovich diamond tip. For each sample, 31 surface indents were done in a load-controlled mode with indentation loads varied between 3 and 45 mN and consequently evaluated based on the Oliver and Pharr method [40]. The Poisson's ratios were taken from [41].

The structure of the as-deposited coatings was investigated by X-ray diffraction (XRD) in Bragg–Brentano configuration using a Panalytical Xpert Pro MPD system equipped with Cu- K_α radiation source ($\lambda = 1.54 \text{ \AA}$). Furthermore, the morphology for selected oxidized samples was investigated using transmission electron microscopy (TEM FEI TECNAI F20) combined with a selected area electron diffraction analysis. Additionally, electron energy-loss spectroscopy (EELS) mappings were performed to determine the elemental chemical composition.

3. Results and discussion

In Table 1 the chemical compositions evaluated by Time-of-Flight Elastic Recoil Detection Analysis (ToF-ERDA) and Rutherford Backscattering Spectrometry (RBS) are summarized for all grown films. The binary $\text{TiB}_{2.57}$ coating shows boron super-stoichiometry, while the B/TM ratio tends to decrease in all the alloyed coatings by increasing the Si content. The lowest total metal content (Ti + TM) of 25 ± 1 at. % was evaluated for the ternary Ti-Si- $\text{B}_{2 \pm z}$ coatings, while the Ti-Ta-Si- $\text{B}_{2 \pm z}$ coatings exhibit nearly 34 ± 1 at. % metal content for both compositions, followed by 30 ± 1 at. % for Ti-Mo-Si- $\text{B}_{2 \pm z}$ coatings. The oxygen content in all grown films is below 2.6 at. %.

Figure 1 presents the X-ray diffractograms of the as-deposited Ti-TM-Si- $\text{B}_{2 \pm z}$ coatings in comparison with the binary $\text{TiB}_{2.57}$. Only peaks corresponding to the hexagonal- TiB_2 phase (SG 191)—in addition to the

Al_2O_3 substrate—can be indexed. Apart from the amorphous $\text{Ti}_{0.20}\text{Mo}_{0.11}\text{Si}_{0.26}\text{B}_{0.43}$, all alloyed coatings exhibit a single-phased hexagonal structure with broad 001 peaks as the preferred orientation. The high Si content in $\text{Ti}_{0.20}\text{Mo}_{0.11}\text{Si}_{0.26}\text{B}_{0.43}$ leads to the amorphous character with diminished peaks. In contrast, the higher Ta-containing $\text{Ti}_{0.28}\text{Ta}_{0.07}\text{Si}_{0.12}\text{B}_{0.53}$ shows an increase in the predominant 001 peak intensity accompanied by a shift towards lower 2θ values, suggesting the dissolution of Ta in the hexagonal phase. Moreover, the calculated c/a ratios are in the range between 1.03 and 1.05. The quaternary systems show slightly lower c/a values compared to the binary $\text{TiB}_{2.57}$ (see Table 1), indicating the substitution of Ti by the dissolved Ta or Mo in the hexagonal lattice.

Moreover, the mechanical properties (surface hardness and Young's modulus) of the coatings are summarized in Table 1. The Ta-alloyed coatings maintained relatively high hardness values with an observed hardening effect by increasing the Ta-Si content from 32.8 to 36 GPa for $\text{Ti}_{0.31}\text{Ta}_{0.04}\text{Si}_{0.06}\text{B}_{0.59}$ and $\text{Ti}_{0.28}\text{Ta}_{0.07}\text{Si}_{0.12}\text{B}_{0.53}$, respectively. The increase in hardness is related to solid solution hardening with Ta addition, which was also reported for other Ta-alloyed borides, i.e. $\text{ZrTaB}_{2 \pm z}$ [42] and $\text{WTaB}_{2 \pm z}$ [43]. In contrast, the Ti-Si and Mo-Si alloying routes lead to decreased hardness with increasing the alloying content. Generally, the alloying of $\text{TiB}_{2 \pm z}$ with Si was emphasized to result in material softening [27,28]. Grančič et al. reported hardness values between 14 and 24 GPa for their amorphous Ti-Si- $\text{B}_{2 \pm z}$ films [28]. The here reported hardness exceeds those values, even at higher Si-contents. This difference is related to the formation of single-phase structured coatings and a predominant 001 orientation—being the preferred one for the anisotropic hardness of hexagonal diborides [8].

Figure 2 summarizes the mass change during dynamic oxidation of Ti-TM-Si- $\text{B}_{2 \pm z}$ coatings as a function of the annealing temperature up to 1400°C. The onset oxidation temperature for the un-alloyed $\text{TiB}_{2.57}$ is observed to be around 490°C. Above this temperature, the coating exhibits a mass increase with accelerated oxidation

Table 1. Chemical composition, crystallographic parameters (c/a ratio), and mechanical properties (H and E) for all grown Ti-(TM)-Si- $\text{B}_{2 \pm z}$ coating materials.

Coating material	Chemical composition [at. %]						B/(Ti + TM)	c/a	H [GPa]	E [GPa]
	Ti	Ta	Mo	Si	B	O				
$\text{TiB}_{2.57}$	27.7	–	–	–	71.2	1.1	2.57	1.054	38.2 ± 3.3	552.0 ± 90.2
$\text{Ti}_{0.25}\text{Si}_{0.08}\text{B}_{0.67}$	23.9	–	–	7.6	65.5	2.6	2.74	1.051	30.4 ± 1.6	443.9 ± 21.5
$\text{Ti}_{0.26}\text{Si}_{0.15}\text{B}_{0.59}$	25.7	–	–	14.2	58.2	1.6	2.26	1.054	23.7 ± 1.0	399.0 ± 21.5
$\text{Ti}_{0.31}\text{Ta}_{0.04}\text{Si}_{0.06}\text{B}_{0.59}$	30.4	3.7	–	6.1	58.4	1.3	1.72	1.032	32.8 ± 2.8	439.7 ± 29.5
$\text{Ti}_{0.28}\text{Ta}_{0.07}\text{Si}_{0.12}\text{B}_{0.53}$	27.7	6.8	–	11.6	52.5	1.3	1.52	1.041	36.0 ± 2.5	434.8 ± 26.1
$\text{Ti}_{0.24}\text{Mo}_{0.05}\text{Si}_{0.12}\text{B}_{0.59}$	23.3	–	5.2	11.6	57.4	2.2	2.01	1.042	27.3 ± 1.0	428.1 ± 10.0
$\text{Ti}_{0.23}\text{Mo}_{0.07}\text{Si}_{0.16}\text{B}_{0.54}$	22.7	–	6.6	16.2	52.2	2.1	1.78	1.034	24.4 ± 0.9	409.1 ± 25.7
$\text{Ti}_{0.20}\text{Mo}_{0.11}\text{Si}_{0.26}\text{B}_{0.43}$	19.8	–	10.3	25.5	42.1	1.8	1.40	–	19.1 ± 1.0	330.9 ± 17.4

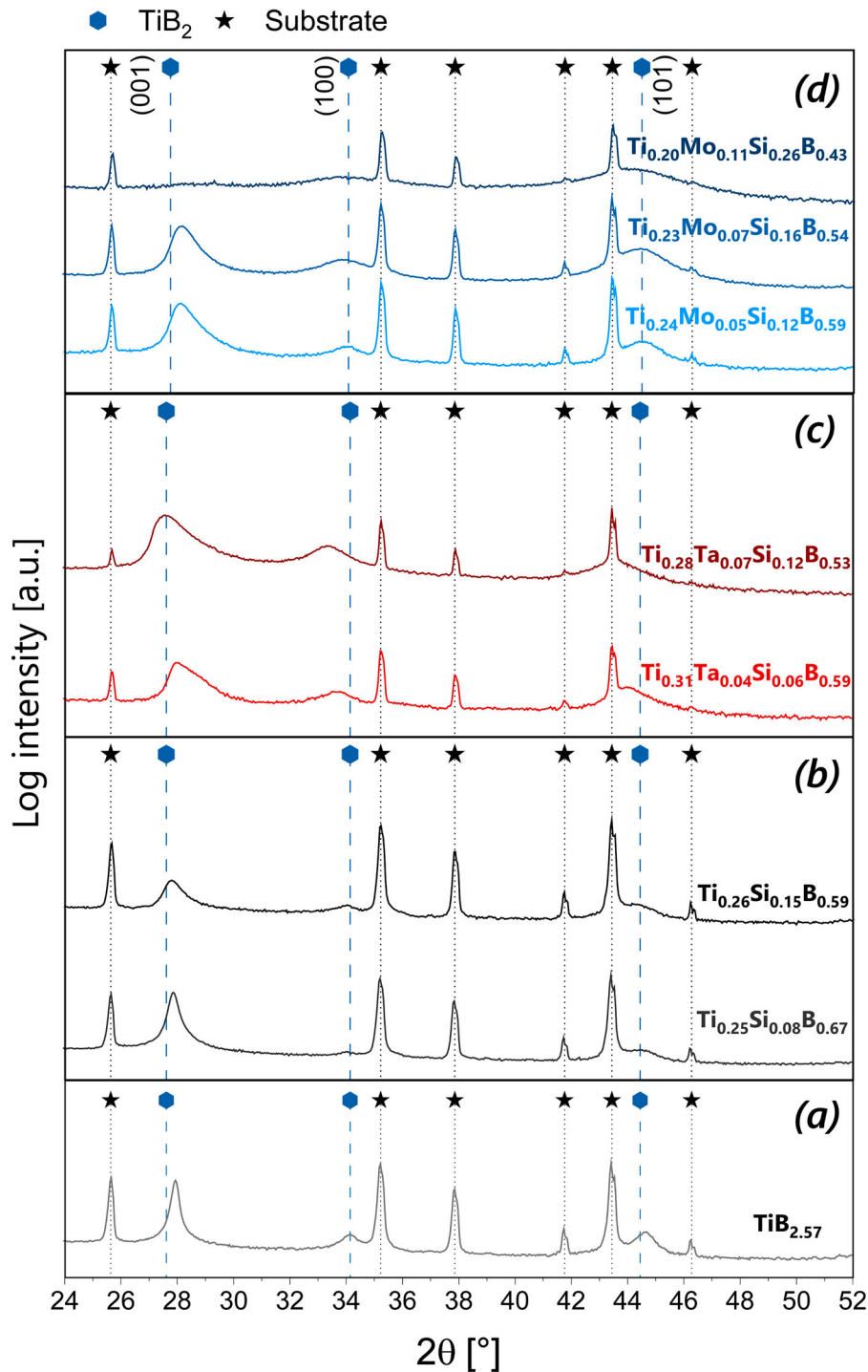


Figure 1. X-ray diffractograms of (a) $\text{TiB}_{2.57}$, (b) $\text{Ti-Si-B}_{2\pm z}$, (c) $\text{Ti-Ta-Si-B}_{2\pm z}$, and (d) $\text{Ti-Mo-Si-B}_{2\pm z}$ alloyed coatings with their stoichiometries indicated.

kinetics till it is fully oxidized at 975°C , followed by a mass decrease above 1000°C due to the volatilization of B_2O_3 . The ternary $\text{Ti-Si-B}_{2\pm z}$ coatings show a slight improvement compared to their binary counterpart with a delayed onset at around 550°C for both $\text{Ti}_{0.25}\text{Si}_{0.08}\text{B}_{0.67}$ and $\text{Ti}_{0.26}\text{Si}_{0.15}\text{B}_{0.59}$ (Figure 2(a)). However, both coatings exhibit the same accelerated oxidation

behavior above the onset temperature and a subsequent evaporation. In contrast, the alloying with Ta-Si provides a clear improvement in the oxidation resistance with a significant shift in the onset temperature up to 770°C for $\text{Ti}_{0.28}\text{Ta}_{0.07}\text{Si}_{0.12}\text{B}_{0.53}$ (see dark-red line in Figure 2(b)). Additionally, the slope of the mass curve reduces significantly till 1000°C —compared to

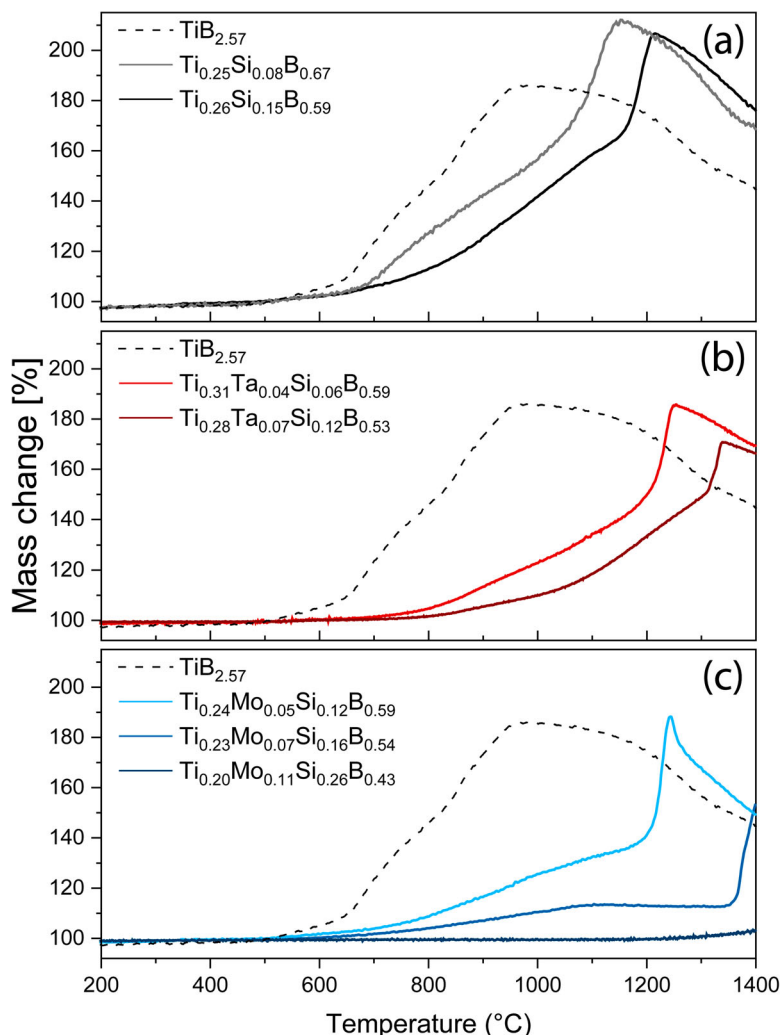


Figure 2. Thermogravimetric (TG) curves of mass change during dynamic oxidation of (a) Ti-Si-B_{2±z}, (b) Ti-Ta-Si-B_{2±z}, and (c) Ti-Mo-Si-B_{2±z} coatings in synthetic air under heating rate of 10°C/min. The TG curve for the binary coating TiB_{2.57} is indicated by a dashed line in (a), (b) and (c).

the binary coating—indicating retarded oxidation kinetics due to the formation of protective scales. Furthermore, the Ti-Mo-Si-B_{2±z} coatings exhibit excellent oxidation resistance, where the slope of the mass gain curves significantly flattens upon alloying. By increasing the Mo-Si content, the mass signal shows a plateau over 1000°C indicating the formation of highly protective oxide scale for both Ti_{0.23}Mo_{0.07}Si_{0.16}B_{0.54} and Ti_{0.20}Mo_{0.11}Si_{0.26}B_{0.43}, respectively. The observed enhancement in oxidation resistance for the quaternary Ti-TM-Si-B_{2±z} coatings is related to a beneficial phase separation of the silicide phases (TaSi₂ and MoSi₂) at around 700°C (also confirmed by XRD analysis, see in supplementary Figure S1), followed by preferential oxidation of Si to form protective Si-based oxide scales, which inhibit oxygen inward-diffusion. MoSi₂ is known as an effective oxidation resistant phase due to the capability to form protective SiO₂ scales, especially

at high temperatures. In contrast, TaSi₂ is reported to exhibit a proper oxidation resistance only up to 800°C, due to competing Ta-based oxides [44,45].

To gain a more detailed understanding on the oxide scale formation process, the morphology of selected oxidized samples was investigated using TEM analysis. Figure 3 presents the cross-sectional TEM analysis for Ti_{0.28}Ta_{0.07}Si_{0.12}B_{0.53} after 1 h oxidation in ambient air at 800°C. The bright-field image shows an oxide scale of 535 nm on top of an unoxidized intact coating featuring columnar morphology (see Figure 3(a)). In more detail, the formed oxide scale is composed of two layers with a distinct interface: an outer dense glassy amorphous layer with a thickness of 140 nm, and an inner layer composed of mixed equiaxed and columnar crystallites (see Figure 3(b)). The inner scale exhibits a relatively dense morphology with small, globular crystallites near to the coating-oxide interface, while more columnar structures

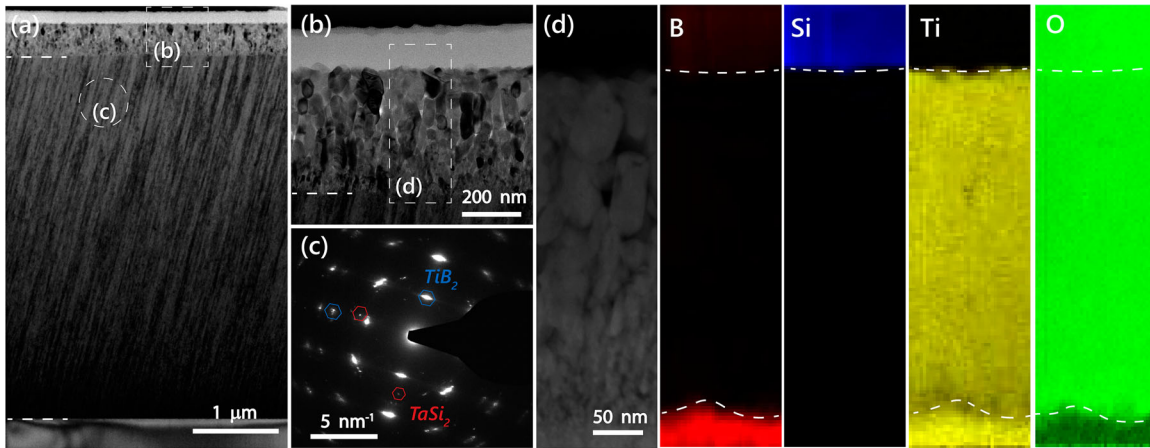


Figure 3. TEM analysis of $\text{Ti}_{0.28}\text{Ta}_{0.07}\text{Si}_{0.12}\text{B}_{0.53}$ coating oxidized in ambient air at 800°C for 1 h. (a) BF image of the whole coating with the substrate at the bottom and oxide scale on top. (b) magnified area of the oxide scale with coating interface. (c) SAED image for the area indicated in (a). (d) STEM image and corresponding EELS maps for the area illustrated in (b).

with larger grains predominate the upper interface. The corresponding EELS maps (see Figure 3(d) and the respective elements) clearly reveal that the outer oxide scale is Si-rich with small amounts of boron, while the inner crystalline scale mainly consists of Ti and Ta-based oxides (Ta is also confirmed by EDX, not shown) with no boron detected. The formation of an outer dense Si-rich borosilicate scale is the key to the excellent oxidation resistance with retarded kinetics. Furthermore, the SAED pattern presented in Figure 3(c) reveals an initiation of phase separation processes between the TiB_2 -based matrix and TaSi_2 after annealing at 800°C .

Figure 4 depicts the TEM analysis for the air-annealed $\text{Ti}_{0.23}\text{Mo}_{0.07}\text{Si}_{0.16}\text{B}_{0.54}$ after 1 h at 1200°C . The unoxidized coating exhibits globular morphology with

clear indications for recrystallization processes as bulk diffusion was already activated at 1200°C —evidence for reaching about 0.4 of the melting temperature [46]—(see Figure 4(a)). Moreover, the BF-image clearly shows a dense oxide scale of 440 nm which is amorphous according to the SAED analysis (see Figures 4(b, c_1)). This coating experienced a separation of the MoSi_2 phase as indicated in SAED image (Figure 4(c_2)) after the annealing at 1200°C . The EELS maps in Figure 4(d) reveal that the oxide scale is based only on Si with no competing boron. However, boron-rich pockets can be observed at the coating-oxide interface due to the formation of MoB phase according to reaction (1). The formation of MoB was reported by Silvestroni et al. for $\text{ZrB}_2/\text{MoSi}_2$ bulk system at 1200°C [30]. Here, the separated MoSi_2 phase

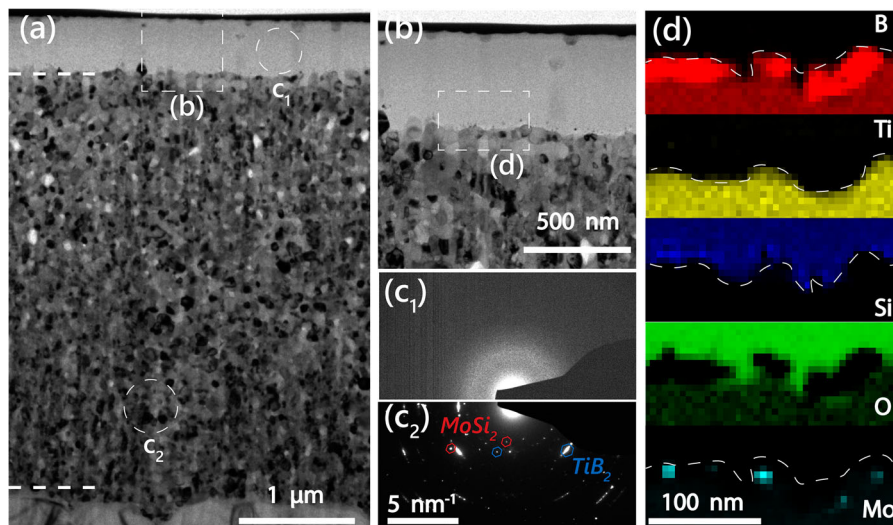
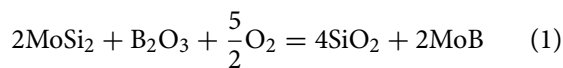


Figure 4. TEM analysis of $\text{Ti}_{0.23}\text{Mo}_{0.07}\text{Si}_{0.16}\text{B}_{0.54}$ coating oxidized in ambient air at 1200°C for 1 h. (a) BF image of the whole coating with the substrate at the bottom and oxide scale on top. (b) magnified area for oxide scale with coating interface. (c_1) and (c_2) SAED patterns for areas indicated in (a). (d) elemental EELS maps for the area illustrated in (b).

beneficially acts as an active reservoir for selective oxidation of Si and the formation of the highly dense and protective Si-based scale, while concomitantly suppressing the detrimental volatile B_2O_3 phase (see equation 1).



To present the best compromise between mechanical properties and oxidation resistance, we correlate in Figure 5 in an uncommon way the as-deposited hardness to the oxidation resistance for selected Ti-(TM)-Si- $B_{2\pm z}$ coatings in relation to literature data. Please note, that the oxidation temperature and the given time refer to an oxidation treatment in air, where a stable and adherent scale was formed. The unalloyed $\text{TiB}_{2\pm z}$ film exhibits high hardness of up to 43 GPa with the lowest onset oxidation temperature of 400°C as reported by Thörnberg et al. [16]—see red star in Figure 5. Increasing the alloying content, in detail Al, the $\text{Ti}_{0.9}\text{Al}_{0.1}\text{B}_{1.3}$ provides an improvement in the oxidation resistance up to 600°C for 10 h, while maintaining a high hardness of 45 GPa [26]. Navidi et al. achieved higher oxidation resistance for their stoichiometric $\text{Ti}_{0.35}\text{Al}_{0.65}\text{B}_{2.0}$ at 700°C, while the high Al-content leads to reduced hardness value of 19 GPa [25]. In comparison, Bakhit et al. employed a lower Al-content to maintain high hardness of 39 GPa for $\text{Ti}_{0.68}\text{Al}_{0.32}\text{B}_{1.35}$ leading also to delayed oxidation kinetics at 800°C for 0.5 h [18]. On the other hand, Grančič et al. reported at 800°C higher scale thickness of 1.2 μm for their alloyed Ti-Si- $B_{2\pm z}$ with 20 at. % Si obtaining only a hardness of 14 GPa [28]. Recently, Glechner et al.

highlighted an outstanding oxidation resistance up to 1100°C in synthetic air for the ternary $\text{Ti}_{0.13}\text{Si}_{0.41}\text{B}_{0.46}$, while the high Si content results also in reduced hardness of 16 GPa [27]. The here described $\text{TiB}_{2\pm z}$ coatings with alloyed TMSi_2 secondary phases exhibit delayed oxidation kinetics compared to their Al-alloyed counterparts, but a higher hardness with respect to the Si-alloyed literature data. This data underlines the need for further alloying concepts, i.e. quaternary diborides. The $\text{Ti}_{0.28}\text{Ta}_{0.07}\text{Si}_{0.12}\text{B}_{0.53}$ coating exhibits delayed oxidation kinetics obtaining a scale thickness of 550 nm after 1 h at 800°C, while featuring a relatively high hardness of 36 GPa in the as-deposited state. Moreover, the Ti-Mo-Si- $B_{2\pm z}$ alloyed coatings show moderate hardness up to 27 GPa, but outperforming all the reported coatings concerning the high-temperature oxidation resistance up to 1200°C due to the formation of protective Si-based scales. The $\text{Ti}_{0.20}\text{Mo}_{0.11}\text{Si}_{0.26}\text{B}_{0.43}$ coating preserved superior oxidation resistance at 1200°C by obtaining thin Si-based scale of 335 nm after 10 h at 1200°C (see in supplementary Figure S2).

4. Conclusions

In this study, novel quaternary Ti-TM-Si- $B_{2\pm z}$ coatings (TM = Mo, Ta) with single-phase AlB_2 structures were deposited by DC magnetron sputtering from alloyed TiB_2 / TMSi_2 targets and investigated in comparison to binary $\text{TiB}_{2\pm z}$ and ternary Ti-Si- $B_{2\pm z}$ coatings. The incorporation of TMSi_2 in TiB_2 yielded mechanically stable quaternary coatings with significantly improved high-temperature oxidation resistance compared to their

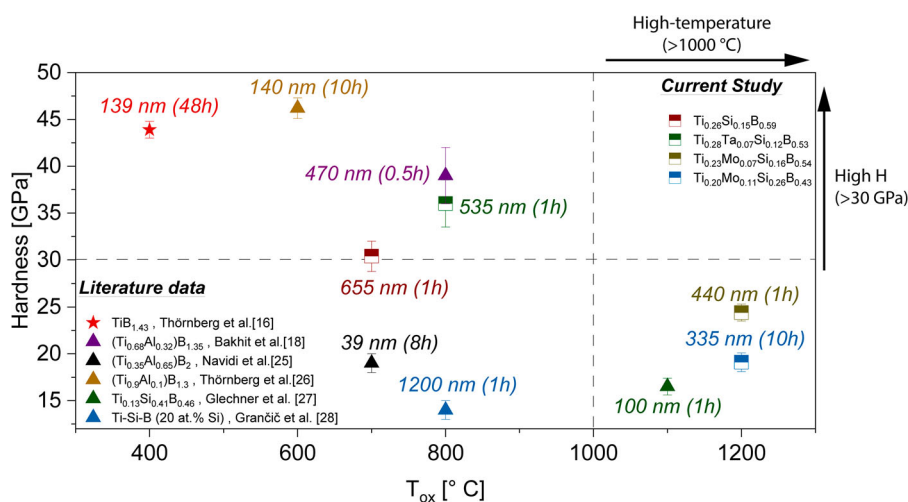


Figure 5. As-deposited hardness of diverse alloyed $\text{TiB}_{2\pm z}$ coatings in relation to their oxidation temperature T_{ox} . The obtained scale thickness (at T_{ox}) for each coating is indicated in relation to the reported oxidation time. The as-deposited coating thicknesses are: 2 μm for $\text{Ti}_{0.26}\text{Si}_{0.16}\text{B}_{0.59}$, 4.9 μm for $\text{Ti}_{0.28}\text{Ta}_{0.07}\text{Si}_{0.12}\text{B}_{0.53}$, 3.5 μm for $\text{Ti}_{0.23}\text{Mo}_{0.07}\text{Si}_{0.16}\text{B}_{0.54}$, 4.9 μm for $\text{Ti}_{0.20}\text{Mo}_{0.11}\text{Si}_{0.26}\text{B}_{0.43}$, 400 nm for $\text{TiB}_{1.43}$ [16], 980 nm for $\text{Ti}_{0.9}\text{Al}_{0.1}\text{B}_{1.3}$ [26], 1.3 μm for $(\text{Ti}_{0.35}\text{Al}_{0.65})\text{B}_2$ [25], ~ 1.5 μm for $(\text{Ti}_{0.68}\text{Al}_{0.32})\text{B}_{1.35}$ [18], and ~ 1.4 μm for $\text{Ti}_{0.13}\text{Si}_{0.41}\text{B}_{0.46}$ [27].

binary and ternary counterparts. The Ti-Ta-Si-B_{2±z} coatings maintained high hardness up to 36 GPa due to solid solution hardening effect of Ta. In addition, the Ti_{0.28}Ta_{0.07}Si_{0.12}B_{0.53} coating exhibited strongly retarded oxidation kinetics at 800°C owing to the formation of an oxide scale with an outer protective glassy Si-rich borosilicate phase. Furthermore, the Ti-Mo-Si-B_{2±z} alloyed coatings preserved an outstanding oxidation resistance up to 1200°C, which is attributed to the selective oxidation of Si and the formation of highly stable and protective Si-based oxide scales, inhibiting oxygen inward diffusion, while suppressing the formation of the detrimental volatile B₂O₃ phase.

The alloying strategy by incorporating TMSi₂ phases into TiB_{2±z} provides a wide playground to stabilize single-phase quaternary Ti-TM-Si-B_{2±z} coatings, featuring remarkable oxidation resistance and good mechanical stability. Nevertheless, the B stoichiometry, as well as high-temperature phase separation processes, need to be considered for further improvements of these novel quaternary diborides.



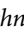
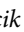


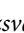


Acknowledgements



The financial support by the Austrian Federal Ministry for Digital and Economic Affairs, the National Foundation for Research, Technology and Development and the Christian Doppler Research Association is gratefully acknowledged (Christian Doppler Laboratory ‘Surface Engineering of high-performance Components’). We also thank for the financial support of Plansee SE, Plansee Composite Materials GmbH, and Oerlikon Balzers, Oerlikon Surface Solutions AG. We also thank the X-ray center (XRC) of TU Wien for beam time as well as the electron microscopy center—USTEM TU Wien—for using the SEM and TEM facilities. Finally, we acknowledge TU Wien Bibliothek for financial support through its Open Access Funding Programme. In addition, the authors thank the RADIATE project for funding our beamtime at the Tandem Laboratory at Uppsala University. Accelerator operation at Uppsala University was supported by the Swedish research council VR-RFI (#2019-00191).

Disclosure statement

No potential conflict of interest was reported by the author(s).

ORCID

Ahmed Bahr  <http://orcid.org/0000-0003-2848-1654>
 Oskar Beck  <http://orcid.org/0009-0004-5307-0595>
 Thomas Glechner  <http://orcid.org/0000-0002-8344-0874>
 Tomasz Wojcik  <http://orcid.org/0000-0001-5091-5215>
 Jürgen Ramm  <http://orcid.org/0000-0001-7314-5938>
 Oliver Hunold  <http://orcid.org/0000-0003-4931-7028>
 Szilard Kolozsvári  <http://orcid.org/0000-0002-3397-7681>
 Peter Polcik  <http://orcid.org/0000-0003-3111-0029>
 Eleni Ntemou  <http://orcid.org/0000-0002-8518-2661>

Daniel Primetzhofer  <http://orcid.org/0000-0002-5815-3742>
 Helmut Riedl  <http://orcid.org/0000-0002-8108-1185>

References

- [1] Fahrenholtz WG, Hilmas GE. Ultra-high temperature ceramics: materials for extreme environments. *Scr Mater*. 2017;129:94–99. doi:10.1016/j.scriptamat.2016.10.018
- [2] Mitterer C. Borides in thin film technology. *J Solid State Chem*. 1997;133(1):279–291. doi:10.1006/jssc.1997.7456
- [3] Chen JS, Wang JL. Diffusion barrier properties of sputtered TiB₂ between Cu and Si. *J Electrochem Soc*. 2000;147(5):1940. doi:10.1149/1.1393462
- [4] Choi CS, Ruggles GA, Shah AS, et al. Stability of TiB₂ as a diffusion barrier on silicon. *J Electrochem Soc*. 1991;138(10):3062–3067. doi:10.1149/1.2085367
- [5] Mayrhofer PH, Mitterer C, Wen JG, et al. Self-organized nanocolumnar structure in superhard TiB₂ thin films. *Appl Phys Lett*. 2005;86(13):131909. doi:10.1063/1.1887824
- [6] Berger M, Hogmark S. Evaluation of TiB₂ coatings in sliding contact against aluminium. *Surf Coat Technol*. 2002;149(1):14–20. doi:10.1016/S0257-8972(01)01361-5
- [7] Polyakov MN, Morstein M, Maeder X, et al. Microstructure-driven strengthening of TiB₂ coatings deposited by pulsed magnetron sputtering. *Surf Coat Technol*. 2019;368:88–96. doi:10.1016/j.surfcoat.2019.04.042
- [8] Fuger C, Hahn R, Hirle A, et al. Revisiting the origins of super-hardness in TiB_{2+z} thin films – impact of growth conditions and anisotropy. *Surf Coat Technol*. 2022;446:128806. doi:10.1016/j.surfcoat.2022.128806
- [9] Yao Y, Zhang Z, Jiao L. Development strategies in transition metal borides for electrochemical water splitting. *Energy Environ Mater*. 2022;5(2):470–485. doi:10.1002/eem2.12198
- [10] Munro RG. Material properties of titanium diboride. *J Res Natl Inst Stand Technol*. 2000;105(5):709–720. doi:10.6028/jres.105.057
- [11] Chen X, Wang H-T, Ji G-C, et al. Microstructure and properties of TiB₂-Ni coatings with different binder phase contents deposited by HVOF spray process. *Rare Met*. 2022;41(4):1385–1393. doi:10.1007/s12598-015-0528-z
- [12] Wu Y, Lu Y, Duan Y, et al. Microstructure and wear properties of powder-pack borided Ti–5Al–2.5Sn alloy. *J Mater Res Technol*. 2023;23:4032–4043. doi:10.1016/j.jmrt.2023.02.052
- [13] Feng Z, Duan Y, Cao Y, et al. Corrosion properties of ceramic coating on pure titanium by pack boronizing with Nd₂O₃. *Ceram Int*. 2023;49(10):15101–15113. doi:10.1016/j.ceramint.2023.01.093
- [14] Hu L-F, Li J, Lv Y-H, et al. Corrosion behavior of laser-clad coatings fabricated on Ti6Al4V with different contents of TaC addition. *Rare Met*. 2020;39(4):436–447. doi:10.1007/s12598-017-0973-y
- [15] Fuger C, Hahn R, Hirle A, et al. Tissue phase affected fracture toughness of nano-columnar TiB_{2+z} thin films. *Mater Res Lett*. 2023;11(8):613–622. doi:10.1080/21663831.2023.2204120
- [16] Thörnberg J, Bakhit B, Palisaitis J, et al. Improved oxidation properties from a reduced B content in

- sputter-deposited TiB_x thin films. *Surf Coat Technol.* **2021**;420:127353. doi:10.1016/j.surfcoat.2021.127353
- [17] Dorri S, Palisaitis J, Greczynski G, et al. Oxidation kinetics of overstoichiometric TiB_2 thin films grown by DC magnetron sputtering. *Corros Sci.* **2022**;206:110493. doi:10.1016/j.corsci.2022.110493
- [18] Bakhit B, Palisaitis J, Thörnberg J, et al. Improving the high-temperature oxidation resistance of TiB_2 thin films by alloying with Al. *Acta Mater.* **2020**;196:677–689. doi:10.1016/j.actamat.2020.07.025
- [19] Tampieri A, Bellosi A. Oxidation of monolithic TiB_2 and of Al_2O_3 - TiB_2 composite. *J Mater Sci.* **1993**;28(3):649–653. doi:10.1007/BF01151240
- [20] Andrievskii RA, Shul'ga YM, Volkova LS, et al. Oxidation behavior of TiB_2 micro- and nanoparticles. *Inorg Mater.* **2016**;52(7):686–693. doi:10.1134/S0020168516070013
- [21] Cai X, Ding S, Wen K, et al. Unmasking the anomalous rapid oxidation of refractory TiB_2 at low temperatures. *J Eur Ceram Soc.* **2021**;41(10):5100–5108. doi:10.1016/j.jeurceramsoc.2021.04.011
- [22] Huang X, Sun S, Tu G. Investigation of mechanical properties and oxidation resistance of CVD TiB_2 ceramic coating on molybdenum. *J Mater Res Technol.* **2020**;9(1):282–290. doi:10.1016/j.jmrt.2019.10.056
- [23] Raju GB, Basu B, Suri AK. Oxidation kinetics and mechanisms of hot-pressed TiB_2 - $MoSi_2$ composites. *J Am Ceram Soc.* **2008**;91(10):3320–3327. doi:10.1111/j.1551-2916.2008.02656.x
- [24] Parthasarathy TA, Rapp RA, Opeka M, et al. A model for the oxidation of ZrB_2 , HfB_2 and TiB_2 . *Acta Mater.* **2007**;55(17):5999–6010. doi:10.1016/j.actamat.2007.07.027
- [25] Kashani N, Mráz AH, Holzapfel S, et al. Synthesis and oxidation behavior of $Ti_{0.35}Al_{0.65}By$ ($y = 1.7$ – 2.4) coatings. *Surf Coat Technol.* **2022**;442:128190. doi:10.1016/j.surfcoat.2022.128190
- [26] Thörnberg J, Mráz S, Palisaitis J, et al. Oxidation resistance and mechanical properties of sputter-deposited $Ti_{0.9}Al_{0.1}B_{2-y}$ thin films. *Surf Coat Technol.* **2022**;442:128187. doi:10.1016/j.surfcoat.2022.128187
- [27] Glechner T, Oemer HG, Wojcik T, et al. Influence of Si on the oxidation behavior of TM -Si- $B_{2\pm z}$ coatings ($TM = Ti, Cr, Hf, Ta, W$). *Surf Coat Technol.* **2022**;434:128178. doi:10.1016/j.surfcoat.2022.128178
- [28] Grančić B, Mikula M, Roch T, et al. Effect of Si addition on mechanical properties and high temperature oxidation resistance of Ti - B - Si hard coatings. *Surf Coat Technol.* **2014**;240:48–54. doi:10.1016/j.surfcoat.2013.12.011
- [29] Raju GB, Biswas K, Basu B. Microstructural characterization and isothermal oxidation behavior of hot-pressed TiB_2 -10wt.% $TiSi_2$ composite. *Scr Mater.* **2009**;61(1):104–107. doi:10.1016/j.scriptamat.2009.03.027
- [30] Silvestroni L, Meriggi G, Sciti D. Oxidation behavior of ZrB_2 composites doped with various transition metal silicides. *Corros Sci.* **2014**;83:281–291. doi:10.1016/j.corsci.2014.02.026
- [31] Silvestroni L, Stricker K, Sciti D, et al. Understanding the oxidation behavior of a ZrB_2 - $MoSi_2$ composite at ultra-high temperatures. *Acta Mater.* **2018**;151:216–228. doi:10.1016/j.actamat.2018.03.042
- [32] Fahrenholtz WG. Thermodynamic analysis of ZrB_2 - SiC oxidation: formation of a SiC -depleted region. *J Am Ceram Soc.* **2007**;90(1):143–148. doi:10.1111/j.1551-2916.2006.01329.x
- [33] Astapov AN, Pogozhev YS, Prokofiev MV, et al. Kinetics and mechanism of the oxidation of $ZrSi_2$ - $MoSi_2$ - ZrB_2 ceramics in air at temperatures up to $1400^\circ C$. *Int J Heat Mass Transf.* **2019**;140:12–20. doi:10.1016/j.ijheatmasstransfer.2019.05.100
- [34] Cao X, Wang B, Ma X, et al. Oxidation behavior of melt-infiltrated SiC - TiB_2 ceramic composites at 500 – $1300^\circ C$ in air. *Ceram Int.* **2021**;47(7, Part A):9881–9887. doi:10.1016/j.ceramint.2020.12.130
- [35] Kiryukhantsev-Korneev P, Sytchenko A, Pogozhev Y, et al. Structure and properties of Zr - Mo - Si - B - (N) hard coatings obtained by d.c. magnetron sputtering of ZrB_2 - $MoSi_2$ target. *Materials (Basel).* **2021**;14(8). doi:10.3390/ma14081932
- [36] Niu Y, Wang H, Liu Z, et al. Microstructure evolution of ZrB_2 - $MoSi_2$ composite coatings at middle and high temperatures. *Surf Coat Technol.* **2015**;273:30–38. doi:10.1016/j.surfcoat.2015.03.029
- [37] Ström P, Primetzhofer D. Ion beam tools for nondestructive in-situ and in-operando composition analysis and modification of materials at the Tandem Laboratory in Uppsala. *J Instrum.* **2022**;17(04):P04011. doi:10.1088/1748-0221/17/04/P04011
- [38] Arstila K, Julin J, Laitinen MI, et al. Potku – New analysis software for heavy ion elastic recoil detection analysis. *Nucl Instrum Methods Phys Res Sect B.* **2014**;331:34–41. doi:10.1016/j.nimb.2014.02.016
- [39] Mayer M. SIMNRA user's guide. 1997.
- [40] Oliver WC, Pharr GM. An improved technique for determining hardness and elastic modulus using load and displacement sensing indentation experiments. *J Mater Res.* **1992**;7(6):1564–1583. doi:10.1557/JMR.1992.1564
- [41] Shein IR, Ivanovskii AL. Elastic properties of mono- and polycrystalline hexagonal AlB_2 -like diborides of s, p and d metals from first-principles calculations. *J Phys: Condens Matter.* **2008**;20(41):415218. doi:10.1088/0953-8984/20/41/415218
- [42] Bakhit B, Palisaitis J, Wu Z, et al. Age hardening in superhard ZrB_2 -rich $Zr_{1-x}Ta_xBy$ thin films. *Scr Mater.* **2021**;191:120–125. doi:10.1016/j.scriptamat.2020.09.026
- [43] Fuger C, Moraes V, Hahn R, et al. Influence of Tantalum on phase stability and mechanical properties of WB_2 . *MRS Commun.* **2019**;9(1):375–380. doi:10.1557/mrc.2019.5
- [44] Berztiss DA, Cerchiara RR, Gulbransen EA, et al. Oxidation of $MoSi_2$ and comparison with other silicide materials. *Mater Sci Eng A.* **1992**;155(1):165–181. doi:10.1016/0921-5093(92)90324-T
- [45] Bahr A, Richter S, Hahn R, et al. Oxidation behaviour and mechanical properties of sputter-deposited $TMSi_2$ coatings ($TM = Mo, Ta, Nb$). *J Alloys Compd.* **2023**;931:167532. doi:10.1016/j.jallcom.2022.167532
- [46] Shewmon PG. Transformations in metals. New York: McGraw-Hill; 1969.